18

Trajectory Studies of NMR Relaxation in Flexible Molecules

RONALD M. LEVY
Rutgers University, Department of Chemistry, New Brunswick, NJ 08903
MARTIN KARPLUS
Harvard University, Department of Chemistry, Cambridge, MA 02138

Stochastic dynamics trajectories for alkanes in aqueous solution have been used to examine a variety of problems that arise in the interpretation of ^{13}C-NMR relaxation experiments. Exact results for spin-lattice and spin-spin relaxation times, and nuclear Overhauser enhancement values obtained from these trajectories, have been employed to analyze the relaxation behavior of small alkanes and macromolecular side chains and to test the validity of simplified relaxation models for these systems. A molecular dynamics simulation of a protein has been used to demonstrate the effects of picosecond fluctuations on observed ^{13}C spin-lattice relaxation times. It is shown how an increase in spin-lattice relaxation time can be related to order parameters for the picosecond motional averaging of the carbon–hydrogen dipolar interactions, and how the order parameters can be calculated from a protein molecular dynamics trajectory. The present work provides a firm theoretical foundation for the continuing effort to use NMR measurements for the experimental analysis of the dynamics of molecules with internal degrees of freedom.

NUCLEAR MAGNETIC RESONANCE RELAXATION MEASUREMENTS provide an important probe of the dynamics of molecules because the spin-lattice (T_1) and spin-spin (T_2) relaxation times and the nuclear Overhauser enhancement (NOE) factor (η) all depend on the thermal motions. For protonated carbons, ^{13}C NMR is particularly well suited for the study of dynamics because the relaxation is dominated by the fluctuating dipolar interactions between ^{13}C nuclei and directly bonded protons. Applications of ^{13}C NMR have been made to the dynamics of small molecules in solution (*1–6*), polymers (*7–13*), and molecules of biological interest including lipids (*14–16*) and proteins (*17–23*). Because the motions of

0065-2393/83/0204-0445$07.00/0
© 1983 American Chemical Society

molecules with many internal degrees of freedom (e.g., macromolecules) are complicated, the interpretation of NMR measurements for such systems is often not unique. Empirical rules have been developed to fit the relaxation data to the molecular tumbling time combined with internal segmental motions (*6–8*). Alternatively, the experimental results have been interpreted in terms of analytically tractable descriptions of the dynamics based on continuous diffusion (*9–24*), restricted diffusion (*25–28*), and lattice jump models (*24, 26, 29, 30*). While it is usually possible to fit the experimental results in this way, the data in themselves generally are not sufficient to determine whether or not a model gives the correct description of the dynamics.

A powerful method of testing relaxation models is provided by computer-generated trajectories that make use of realistic potentials to simulate the motion of the system of interest. From such trajectories, the time-dependent correlation functions can be determined and T_1, T_2, and η can be calculated. Thus the trajectory provides simultaneously a complete knowledge of the dynamics and exact values of the NMR parameters. It is now possible to proceed by using the calculated values of T_1, T_2, and η as "experimental" quantities and fitting the various models to them. The resulting model dynamics can then be compared with the exact dynamics from the trajectory to determine how well the former corresponds to the latter. Also, the results of the trajectory studies may be compared directly with experiment without recourse to simplified theories.

In this chapter we review our work, which employs the results of computer simulations for the analysis of experimental and theoretical NMR studies of the motions of flexible molecules. The systems considered include butane and heptane tumbling in aqueous solution and the short- and long-time dynamics of side chains attached to macromolecules. The first section of this chapter reviews the procedures used to generate the trajectories and outlines the methodology employed to extract the NMR parameters from them. Then the butane and heptane trajectories are used, in the next section, to evaluate the relaxation times for these alkane chains in the motional narrowing limit, and the results are compared with experiment and with simplified models. The following section analyzes the dynamics of a side chain protruding from a macromolecule and employs the heptane trajectories to critically examine a lattice jump model for the relaxation. In the final section we make use of a full molecular dynamics simulation of a protein to demonstrate the effects of fast protein motions on observed ^{13}C-NMR relaxation times.

Methodology

In this section we outline the method used for obtaining the alkane trajectories and present the procedure for determining NMR relaxation

parameters from these trajectories. We show how trajectory results can be applied to study simplified dynamical models that have been used to interpret NMR relaxation data. For the analysis of ^{13}C spin lattice relaxation in proteins we show how an increase in the relaxation time is related to order parameters for the picosecond motional averaging of the $^{13}C,H$ dipolar interactions, and how these order parameters are calculated from a molecular dynamics trajectory.

Diffusive Langevin Dynamics of Model Alkanes. The equation of motion descriptive of Brownian particles is the Langevin equation (*31*)

$$m_i \frac{d\boldsymbol{v}_i}{dt} = -\zeta_i \boldsymbol{v}_i + \boldsymbol{F}_i + \boldsymbol{A}_i \tag{1}$$

where $m_i \boldsymbol{v}_i$, and ζ_i are the mass, velocity, and friction constant of the ith particle and $\boldsymbol{F}_i$ is the systematic force acting on the ith particle due to the potential of mean force; $\boldsymbol{F}_i$ in general depends on the coordinates of all the particles. The stochastic term $\boldsymbol{A}_i(t)$ represents the randomly fluctuating force on the particle due to the solvent. In the diffusive regime, the particle momenta relax to equilibrium much more rapidly than the displacements. With the assumption that the forces are slowly varying, i.e., that it is possible to take time steps that are large compared to the momentum relaxation time $\left(\Delta t >> \frac{m_i}{\zeta_i}\right)$, Equation 1 can be integrated to obtain the equation (*31–33*) for the displacement vector, $\boldsymbol{r}_i$

$$\boldsymbol{r}_i(t + \Delta t) = \boldsymbol{r}_i(t) + [\boldsymbol{F}_i(t)/\zeta_i]\Delta t + \Delta \boldsymbol{r}_i(t) \tag{2}$$

The term $\Delta \boldsymbol{r}_i(t)$ is the random displacement due to the stochastic force; it is chosen from a Gaussian distribution with zero mean and second moment $6D_i\Delta t$, where D_i, the diffusion coefficient, is KT/ζ_i.

Equation 2 is the equation used to calculate the trajectories of the hydrocarbon chains (*34*). An extended-atom model was introduced, in which the CH_3 and CH_2 units are represented as spheres of van der Waals radius 1.85 Å; the bond lengths and angles of the alkane chains were set equal to 1.523 Å and 111.3°, respectively. Each extended-atom group along the chain acted as a point center of frictional resistance with a Stokes' law friction constant $\zeta_i = 6\pi\eta a$. To determine η, the viscosity of water at 25 °C ($\eta = 0.01$ poise) was used and a was set equal to the extended-atom van der Waals radius; with these parameters, $\zeta_i = 3.45 \times 10^{-9}$ g/s. This is to be compared with the value of $\zeta_i = 2.2 \times 10^{-9}$ g/s obtained from the experimental diffusion coefficient of methane in water at 25° C.

POTENTIAL FUNCTION. The negative gradient of the potential of mean force is used for $\boldsymbol{F}_i$ in Equations 1 and 2. This is a combination of

the potential energy arising from the interactions among the particles composing the solute molecule and the effective potential due to the solvent molecules. The molecular potential was expressed as a sum of two types of terms; the first is a torsional potential energy for each of the dihedral angles, and the second consists of pairwise Lennard–Jones interactions between extended atoms separated by four or more bonds (*35, 36*). For butane there is one angular degree of freedom and only the associated torsional potential was used, but for heptane both torsional and nonbonded terms are required.

The solvent contribution to the torsional nonbonded potential was obtained from the work of Pratt and Chandler (*3*), which expresses the potential due to the solvent as $-kT \ln (y)$ where y is the cavity distribution function. The differences in energy at 25 °C between the *trans* and *gauche* butane geometry in the vacuum and in the solvent are 0.70 kcal/mol and 0.16 kcal/mol, respectively. For the solvent effect on the nonbonded interaction, the cavity distribution function for two methane molecules dissolved in water was used (*37*). The solvent-modified potential has a slightly deeper energy minimum (-0.38 versus -0.30 kcal/mol), which occurs at a smaller interparticle separation (3.0 versus 4.15 Å); at larger separations the attraction is more quickly screened in the solvent.

For all the systems considered, Equation 2 was integrated in Cartesian coordinates with the bond lengths and angles of the molecule constrained to the initial value by use of the SHAKE algorithm (*35*). In general, a correction term should be introduced when the Langevin equation is solved with constraints (*38*). This term was omitted from the present simulation, in which the effect is expected to be small (*39*).

For the butane simulation, time steps of 0.005 ps and 0.05 ps were compared; for the other molecules, time steps between 0.025 and 0.05 ps were used. Butane trajectories were run for 90 ns (25 °C) and 20 ns (50 °C) on the solvent-modified potential surface and 20 ns (25 °C) on the vacuum molecular potential surface. Heptane trajectories on the solvent-modified surface (25 °C) were recorded for 20 ns without constraints and for 10 ns with three atoms held fixed. For 10 ns of the butane trajectory (0.05-ps time step), the required central processing unit time on an IBM 370/168 computer was 15 min.

Exact Calculation of NMR Parameters. The NMR relaxation parameters probe angular correlation functions of the relaxing nucleus. These correlation functions and their Fourier transforms, the spectral densities, can be obtained directly from the alkane trajectories, which provide the complete chain dynamics in the diffusive limit. For the ^{13}C nucleus in an alkane chain, the dynamical quantities of interest are the spherical polar coordinates (with respect to a laboratory frame) of the C–H internuclear vectors. The well-known relations between the NMR

relaxation parameters T_1, T_2, and η and the spectral densities for the case of dipolar relaxation involving two different spin 1/2 nuclei (*40*) are

$$\frac{1}{T_1} = \frac{N\hbar^2\gamma_C^2\gamma_H^2}{r^6}\frac{4\pi}{10}\{J_0(\omega_C - \omega_H) + 3J_1(\omega_C) + 6J_2(\omega_C + \omega_H)\} \quad (3)$$

$$\frac{1}{T_2} = \frac{N\hbar^2\gamma_C^2\gamma_H^2}{r^6}\frac{4\pi}{20}\{4J_0(0) + J_0(\omega_C - \omega_H) + 3J_1(\omega_C) + 6J_1(\omega_H) + 6J_2(\omega_C + \omega_H)\} \quad (4)$$

$$\eta = \frac{\gamma_H}{\gamma_C}\left[\frac{6J_2(\omega_C + \omega_H) - J_0(\omega_C - \omega_H)}{J_0(\omega_C - \omega_H) + 3J_1(\omega_C) + 6J_2(\omega_C + \omega_H)}\right] \quad (5)$$

where γ_C, γ_H and ω_C, ω_H are the gyromagnetic ratios and Larmor frequencies of the ^{13}C and ^1H nuclei, r is the C–H bond distance, and N is the number of protons directly bonded to the relaxing carbon nucleus. The spectral densities, $J_m(\omega)$, are the Fourier transforms of the second-order spherical harmonics, $Y_m^2(\theta, \phi)$ given by

$$J_m(\omega) = \int_0^\infty \langle Y_m^2[\theta(t)\phi(t)]\ Y_m^{*2}\ [\theta(0)\phi(0)]\rangle \cos \omega t\, dt \quad (6)$$

where the spherical-harmonic time correlation function is defined as the ensemble average

$$\langle Y_m^2[\theta(t)\phi(t)]Y_m^{*2}[\theta(0)\phi(0)]\rangle = \int d\theta d\phi \int d\theta' d\phi'\ Y_m^2(\theta, \phi)\ G(\theta, \phi, t; \theta', \phi', 0)Y_m^{*2}(\theta'\phi') \quad (7)$$

Here $G(\theta, \phi, t; \theta', \phi', 0)$ is the conditional probability that a CH vector has spherical polar coordinates $(\theta\phi)$ at times t, given that they were equal to $(\theta'\phi')$ at time 0. The spherical-harmonic time correlation functions are obtained from the alkane trajectories by replacing the ensemble average (Equation 7) with a time average (*41*). Since the orientation of the laboratory z axis is arbitrary for freely rotating molecules, the angular correlations and their spectral densities are independent of subscript m.

Once the correlation functions (Equation 7) have been evaluated from the time integral over the trajectory, the spectral densities are obtained by numerical Fourier transformation, as indicated in Equation 6. The resulting values of $J_m(\omega)$ are then introduced into Equations 3–5 to determine the NMR parameters.

Relaxation Models. The ^{13}C-NMR spectra of low molecular weight species in solution have tumbling times that are much smaller than the reciprocal of the Larmor frequencies of current spectrometers. Consequently, the resonances of such systems are observed in the motional narrowing limit $(\omega_C\tau)^2 << 1$, where the relaxation time τ is the time integral of the angular correlation function

$$\tau \equiv \int_0^\infty \langle Y_m^2[\theta(t)\phi(t)]\ Y_m^{*2}\ [\theta(0)\phi(0)]\rangle\ dt \tag{8}$$

In the motional narrowing limit, the NMR relaxation times T_1 and T_2 are equal and independent of the Larmor frequency and the ^{13}C dipolar NOE is maximal (*1*, *40*); that is, Equations 3–5 reduce to

$$\frac{1}{T_1} = (4\pi\tau)\frac{N\hbar^2\gamma_C^2\gamma_H^2}{r^6} \tag{9}$$

$$T_2 = T_1 \tag{10}$$

$$\text{NOE} = 1 + \eta = 2.99 \tag{11}$$

For rigid spherical molecules in solution, the rotational motion is described by the angular Debye diffusion equation and the second-order spherical harmonics decay as a single exponential (*41*) with relaxation time $\tau = 1/(6D)$, where D is the rotational diffusion coefficient. For flexible molecules, a distribution of relaxation times is required to describe the motion of a given C–H vector. For liquid alkanes, an effective relaxation time τ_{eff} has been extracted from experimental T_i values; τ_{eff} may be thought of as a weighted average of the distribution of relaxation times. Empirically, τ_{eff} has been separated into contributions from molecular tumbling and segmental motions (*6*, *10*, *11*)

$$\frac{1}{\tau_{eff}} = \frac{1}{\tau_0} + \frac{1}{\tau_i} \tag{12}$$

where τ_0 is the molecular tumbling time, and τ_i is the segmental motion relaxation time for the ith carbon. To test the validity of Equation 12 using the alkane trajectories, we have considered a local coordinate system centered on the relaxing nucleus and analyzed its motion relative to a coordinate frame embedded in the molecule (*41*). To express the angular correlation functions (Equation 7) in terms of these coordinate systems we use the Wigner rotation matrices D_{ma}^2, which transform the spherical harmonics between coordinate frames related by the Euler

angles Ω. The resulting expression is

$$\langle Y^2_m[\theta(t)\phi(t)]\ Y^{*2}_{m'}[\theta(0)\phi(0)]\rangle$$
$$= \sum_{\substack{aa' \\ bb'}} \langle [D^{*2}_{ma}(\Omega_0(t))\ D^2_{ma'}\ (\Omega_0(0))]\ [D^{*2}_{ab}(\Omega_i(t))\ D^2_{a'b'}(\Omega_i(0))]\rangle$$
$$\times\ Y^2_b(\theta_{\text{mol}},\ \phi_{\text{mol}})\ Y^{*2}_{b'}(\theta_{\text{mol}},\ \phi_{\text{mol}}) \tag{13}$$

Where $D^2_{ab}(\Omega)$ is the Wigner rotation matrix, $\Omega_0(t)$ are the Euler angles for the transformation from the laboratory to the molecular coordinate system, and $\Omega_i(t)$ are the Euler angles for the transformation from the molecular coordinate system to the local coordinates centered on the ith relaxing nucleus. The angles $(\theta_{\text{mol}},\ \phi_{\text{mol}})$ are the time-independent spherical polar coordinates of the C–H internuclear vector in the local coordinate system. An expression of the form of Equation 12 for τ_{eff} can be obtained with the assumptions that tumbling and internal motions are independent, and that the correlation functions describing the tumbling and internal motions decay as a single exponential. For this situation, the correlation functions of Equation 13 can be broken into a sum over products of correlation functions of the form:

$$\langle D^{*2}_{ma}[\Omega_0(t)D^2_{ma'}(\Omega_0(0)]\rangle \simeq e^{-t/\tau_0}\delta_{aa'} \tag{14a}$$

$$\langle D^{*2}_{ab}[\Omega_i(t)]D^2_{ab'}[\Omega_i(1)]\rangle \simeq e^{-t/\tau_i}\delta_{bb'} \tag{14b}$$

Substitution of this result into Equation 13 permits one to obtain an expression of the form of Equation 12 for τ_{eff}. In the next section of this chapter we employ the stochastic trajectory results for butane and heptane to evaluate the correlation functions (Equation 13), compare calculated NMR relaxation times with experimental trends for liquid alkanes, and analyze the validity of the approximations inherent in Equation 12 and Equations 14a and 14b.

More realistic models of NMR relaxation in polymers take into account the presence of torsional barriers and of excluded volume effects. One type of analytic model, which has been applied to hydrocarbon chains in membranes and in solution, is the so-called *jump model* (*26, 27*). In practice, there have been few attempts to interpret experimental NMR relaxation data within the context of a complete lattice jump model because the number of adjustable parameters rapidly becomes unwieldly. For the hydrocarbon relaxation problem, it has been common to employ the model with the product approximation for the relaxation; this omits excluded volume effects and the possibility of concerted motions. Each carbon–carbon bond is allowed to jump between three states, *trans*,

gauche (+), and *gauche* (−). The rate constant for jumping from the *trans* (τ) to *gauche* (g^+, g^-) states is K_T, and the inverse rate constant is K_G. For this simplified lattice jump model the correlation functions for each of the internal degrees of freedom (Equation 13) can be written as a sum over the conditional probabilities for the allowed transitions in the form (*24, 29, 41*)

$$\langle D^{*2}_{ab}[\Omega(t)]D^{2}_{a'b'}[\Omega(0)]\rangle = d^2_{ab}(\beta)d^2_{a'b'}(\beta)\sum_{\phi=\tau,\ g^-,g^+}\ \sum_{\phi=\tau,g^-,g^+} e^{i[b\phi-b'\phi']}\,P_0(\phi')P(\phi t|\phi' 0) \quad (15)$$

The d^2_{ab} terms are real reduced Wigner matrix elements, with β the complement of the rigid CCC bond angle, $P(\phi t|\phi' 0)$ is the conditional probability that a rotational angle is ϕ at time t, given that it was ϕ' at time 0, and $P_0(\phi')$ is the equilibrium probability of a ϕ' state. Explicit expressions for the conditional probabilities are derived in terms of the eigenvalues and eigenvectors of the rate matrix (*29, 41*).

The lattice jump model is studied in some detail later in this chapter. The heptane trajectory is used to evaluate T_1, T_2, and NOE for a model amino acid side chain with four internal rotational angles. Figure 1 shows the four rotational angles and indicates the nature of the three types of coordinate systems that are used to define the configurations of the chain; that is, the laboratory system, the macromolecular system with respect to which the overall tumbling is defined, and the four local coordinate frames associated with the internal degrees of freedom. For the analysis, the coordinate frame centered on C2 is assumed to be rigidly attached to the macromolecule, which is tumbling isotropically with relaxation time τ_0. Only carbons C2 through C6 are considered, because the C7 methyl protons cannot be located from an extended-atom alkane model. The NMR parameters calculated exactly from the trajectory are compared with those obtained from the independent lattice jump model. For the latter, only the isomerization rate constants K_T and K_G for each of the rotational angles are required (*34, 43*).

Another class of NMR relaxation problems for which excluded volume effects are important deals with the contribution of fast (picosecond) motions to the relaxation of amino acid side chains in the interior of proteins (*21–29*). In the last section of this chapter we review our use of a full molecular dynamics simulation of the protein pancreatic trypsin inhibitor (PTI) to demonstrate the effects of picosecond fluctuations on observed ^{13}C T_i values. The protein trajectory has been used to evaluate the short time decay of internal correlation functions (Equation 14b), which determine the NMR relaxation (*44–45*). Because of the highly restricted nature of the motion in the protein interior, the internal correlation functions generally do not decay to zero. Instead, a plateau value

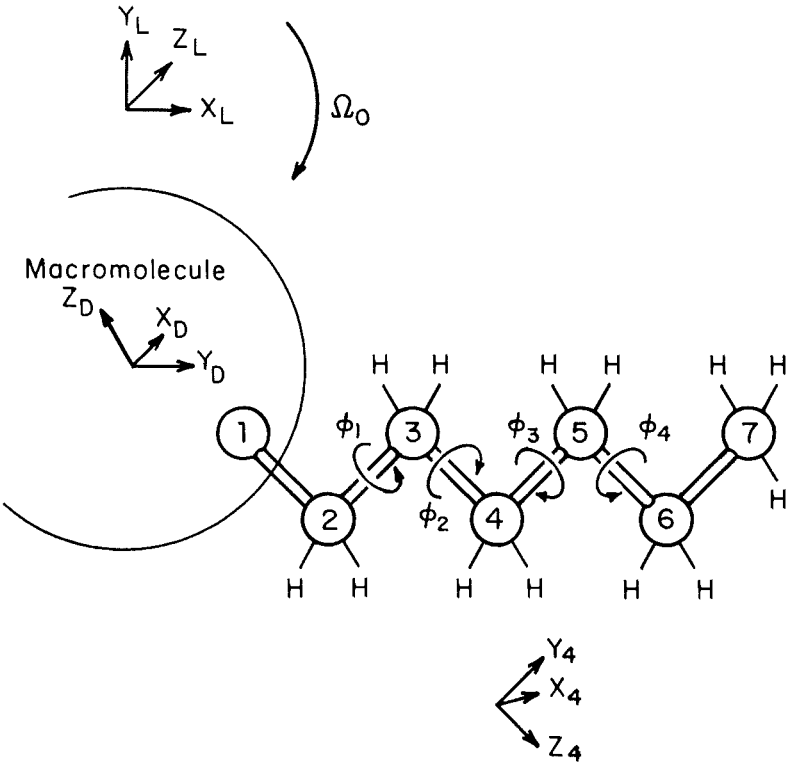

Figure 1. Schematic representation of a side chain with four internal rotational angles attached to a tumbling macromolecule. The laboratory coordinate system, molecular tumbling coordinate system, and a coordinate system attached to C4 are labeled. (Reprinted from Ref. 4. Copyright 1981, American Chemical Society.)

is often reached after t_p picoseconds, where t_p is a time short compared with the length of the trajectory. We have previously shown that, for such a plateau value, the internal correlation function is equal to the equilibrium orientation distribution obtained from the entire run (*45, 46*)

$$(\mathcal{S}_j)^2 = \frac{4\pi}{5} \sum_a | \langle Y_{a1}^2[\theta_j(t)\phi_j(t)]\rangle|^2 \tag{16}$$

The quantity $\mathcal{S}_j$ defined by Equation 16 is the generalized order parameter for the restricted motion of the internuclear dipole vector (*45–48*). The carbon relaxation, corrected for the picosecond motional averaging

of the internuclear dipole vector, is

$$T_{1j} \simeq \mathcal{S}^{-2}\, T_{1j}^{R} \tag{17}$$

where the rigid relaxation time, T_{1j}^{R} is calculated from Equation 3 with

$$J(\omega) = \frac{1}{4\pi} \frac{\tau_0}{1 + (\omega\tau_0)^2} \tag{18}$$

In a later section we review our results concerning the evaluation of order parameters from protein trajectories and show that under suitable conditions, ^{13}C-NMR relaxation data can serve to probe the picosecond reorientation dynamics of the C–H bond vector.

NMR Relaxation of Model Alkanes in the Motional Narrowing Limit

In this section we employ the stochastic trajectory results for butane and heptane to analyze the contributions to the ^{13}C relaxation times in simple alkanes. The calculated relaxation times are compared with experimental trends. We also examine some simplified models that have been proposed for interpreting alkane NMR data and test them by comparison with the trajectory results.

Relaxation Time: Theory and Experiment. In the motional narrowing limit applicable to the small alkanes, the ^{13}C dipolar spin lattice relaxation times (T_1; see Equation 9) are inversely proportional to the relaxation times (τ) of the second-order spherical harmonics. The computed relaxation times for each of the internuclear vectors of butane and heptane, obtained from a least-squares fit of a single exponential to the decay of the calculated correlation functions, are listed in Tables I and

Table I. Relaxation Times of Butane Angular Correlation Functions

Bond	$\langle Y_0^{*1}(0)Y_0^1(t)\rangle$ $\tau(ps)$	$\langle Y_0^{*2}(0)Y_0^2(t)\rangle$ $\tau(ps)$	$\langle Y_1^{*2}(0)Y_1^2(t)\rangle$ $\tau(ps)$	$\langle Y_2^{*2}(0)Y_2^2(t)\rangle$ $\tau(ps)$
C1–C2	(18.5)[a] 16.0	5.7	5.6	5.8
C2–C3	(19.1) 16.9	6.1	5.9	6.4
C3–C4	(19.0) 15.9	6.0	5.6	5.8
C2–H	(7.6)[b] 8.1	(3.9)[b] 5.0	(4.0)[b] 4.9	(3.9)[b] 5.1
C3–H	(7.8) 8.3	(4.1) 5.2	(3.9) 4.8	(3.9) 5.1

Note: Relaxation time from least-squares fit of the relaxation to a single exponential over 10 ps, except as noted.

[a] Least-squares fit to single exponential over 20 ps.

[b] Least-squares fit to single exponential over 5 ps.

Table II. Relaxation Times of Heptane Angular Correlation Functions

Bond	$\langle Y_0^{*1}(0)Y_0^1(t)\rangle$ $\tau(ps)$	$\langle Y_0^{*2}(0)Y_0^2(t)\rangle$ $\tau(ps)$	$\langle Y_1^{*2}(0)Y_1^2(t)\rangle$ $\tau(ps)$	$\langle Y_2^{*2}(0)Y_2^2(t)\rangle$ $\tau(ps)$
C1–C2	(39.3)[a] 33.4	13.4	14.7	15.9
C2–C3	(46.7) 42.2	16.5	15.1	16.5
C3–C4	(51.9) 49.8	17.6	19.6	20.2
C4–C5	(50.3) 46.7	18.1	16.9	18.3
C5–C6	(47.3) 41.6	16.5	17.2	18.3
C6–C7	(37.3) 35.7	13.7	12.9	13.5
C2–H	(32.6)[a] 29.1	12.6	11.7	11.9
C3–H	(31.5) 29.4	13.9	11.3	13.5
C4–H	(35.1) 33.1	15.1	11.6	13.3
C5–H	(33.8) 33.4	13.4	12.3	12.5
C6–H	(25.4) 23.3	9.9	12.9	12.7

Note: Relaxation time from least-squares fit of the relaxation to a single exponential over 10 ps, except as noted.

[a] Fit to a single exponential over 20 ps.

II, respectively. Since the relaxation is not due to isotropic rigid body rotation, the single exponential fit is approximate. In Table III we compare the relaxation times obtained from a single exponential fit to the C6–H vector in heptane with the results from the time integral of the angular correlation function (Equation 8). For the complete dynamics (top row of results), the time integral of the correlation function gives a value for the relaxation time about 14% smaller than that estimated from a single exponential fit. Such a difference is not important for the analysis described below.

The relaxation times listed in Tables I and II demonstrate a number of important trends. They can be summarized as follows:

1. The relaxation times for these small alkanes in water, whose overall tumbling puts them in the motional narrowing limit, are typically between 5 and 50 ps.
2. The relaxation times increase as the chain length increases from butane to heptane.
3. The relaxation times increase from the ends of the heptane chain toward the center.
4. The relaxation of the Y_0^1 correlation functions are always slower than that of the Y_M^2 functions, but the ratio of $\tau_{l=1}/\tau_{l=2}$ is less than three.
5. The C–H internuclear vectors relax faster than the C–C vectors.

Table III. Time Integral of Angular Correlation Function of C6–H Vector and Exponential Relaxation Times

	$\int_0^\infty \langle Y_0^2[\theta(0)\phi(0)]Y_0^2[\theta(t)\phi(t)]\rangle dt$ (ps)	*Relaxation Time by Single Exponential Fit (ps)*
Complete dynamics	0.68	9.9[a] (0.79)[b] 10.5[c] (0.84)
Tumbling and internal motions uncoupled	0.58	9.7[a] (0.77) 11.7[c] (0.93)
Tumbling relaxation only	1.21	13.0[a] (1.03) 15.8[c] (1.26)
Internal relaxation only	—	39[c] (3.1) 40.1[d] (3.2)

[a] Least-squares fit to a single exponential over 10 ps.
[b] Values in parentheses are $1/4\pi$ times the exponential fit to correspond to the time integral (Equation 8).
[c] Least-squares fit to a single exponential over 20 ps.
[d] Least-squares fit to a single exponential over 50 ps.

The first three results are in accord with experiment; there are no data concerning the final two.

From the C–H relaxation times listed in Tables I and II, the ^{13}C-spin-lattice relaxation times (T_1) are calculated by means of Equation 9. Table IV lists the predicted ^{13}C T_1 values for each of the methylene carbons of butane and heptane; the final column gives the ratio of T_1 for carbon C2 and the ith internal carbon. Unfortunately, experimental measurements of these relaxation times for small alkanes in aqueous solution are not available. However, measurements of T_1 values have been reported for neat liquid alkanes (*10, 11*), and some of these results are given in Table IV. Quantitative comparison of the heptane results shows that the T_1 values calculated from the trajectories are shorter than the experimental results by a factor of six. One source of this difference is in the larger viscosity of the aqueous solution relative to the neat liquids. The viscosities of the neat alkanes at the experimental temperature of 40 °C are three to four times smaller than the viscosity used for the aqueous solution calculation (η = 0.27 centipoise for hexane at 40 °C, η = 0.34 centipoise for heptane at 40 °C, compared with η = 1 centipoise for aqueous solution). If we assume the trajectory results scale linearly with the viscosity (as they are expected to do in the diffusive limit), we find that the calculated relaxation times for heptane are a factor of 1.5–2 shorter than the experimental values. Differences of this order may be due to the limitations of the stochastic dynamics model (*34*); these include the neglect of the inertial term of the complete Langevin equa-

Table IV. Alkane NMR Spin-Lattice Relaxation Times

	T_1 (s)	T_1^{C2}/T_1^{Ci}
	Trajectory Results[a]	
Butane carbons		
C2, C3	5.9 ± 0.12	
Heptane carbons		
C2, C6	1.94 ± 0.18	—
C3, C5	1.82 ± 0.14	1.07
C4	1.75 ± 0.24	1.11
	Experimental Results[b]	
Heptane carbons		
[C1, C7]	[10.9]	[0.81[c]]
C2, C6	13.2	—
C3, C5	12.8	1.03
C4	12.0	1.10
Eicosane carbons		
[C1, C20]	[3.6]	[0.43[c]]
C2, C19	2.3	—
C3, C18	1.6	1.44
C4, C17	1.1	2.09
Interior[d]	0.8	2.88

[a] 25 °C, η = 1 centipoise, aqueous solution.
[b] 39 °C, η = 0.34 centipoise for neat heptane (*10*).
[c] Normalized to the same number of directly bonded protons.
[d] Individual values not obtained.

tion, the neglect of hydrodynamic interaction, and the use of an atomic friction coefficient obtained from the translational diffusion coefficient of a monomer unit in the Langevin equation for the alkane chain. In this regard, if the covalent radius (0.77 Å) is used to obtain the monomer friction coefficient, as has been suggested (*49*), the calculated T_1 values are increased by 2.4 and are closer to experimental values. It is important to note that, while the absolute values of the predicted T_1 values are somewhat too short, the trajectory results reproduce the experimentally observed gradient in the values of T_1 along the heptane chain.

Test of Simplified Models. To explore whether relaxation in the motional narrowing limit can be divided into contributions from tumbling and segmental motions, the relaxation of the C6 carbon of heptane was analyzed. The molecular tumbling axis of the heptane molecule was defined by atoms C1–C2–C3. Both the tumbling correlation function and the correlation functions describing the internal relaxation were calculated directly from the trajectory. Figure 2 compares the decay of the second-order spherical harmonics of the C6–H internuclear vector cal-

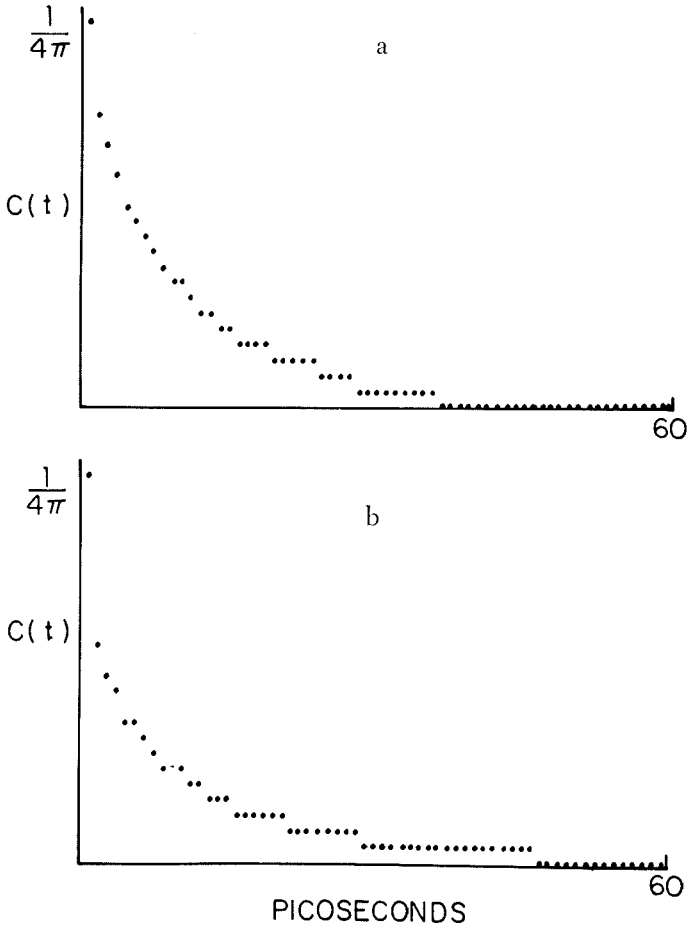

Figure 2. Relaxation of the second-order spherical harmonics $\langle Y^2_0(\theta(t)\phi(t)) \times Y^2_0(\theta(0)\phi(0))\rangle$ *of the C6–H internuclear vector calculated from the heptane trajectory. (a) Exact results from trajectory (Equation 13). (b) Results when correlations between tumbling and internal motions are broken (Equation 14a). (c) Relaxation of diagonal tumbling correlation function,* $\frac{1}{4\pi}\sum_a \langle D^{*2}_{ma}(\Omega_0(t))\, D^2_{ma}(\Omega(0))\rangle$ *in Equation 14a. (d) Relaxation of internal correlation function,* $\frac{1}{5}\sum_{bb'} \langle D^{*2}_{ab}(\Omega_i(t))\, D^2_{ab'}(\Omega_i(0))\rangle\, Y^2_b(\theta_{mol}\phi_{mol})\, Y^{*2}_{b'}(\theta_{mol}\phi_{mol})\rangle$, *in Equation 14b. (Reprinted from Ref. 41. Copyright 1981, American Chemical Society.)*

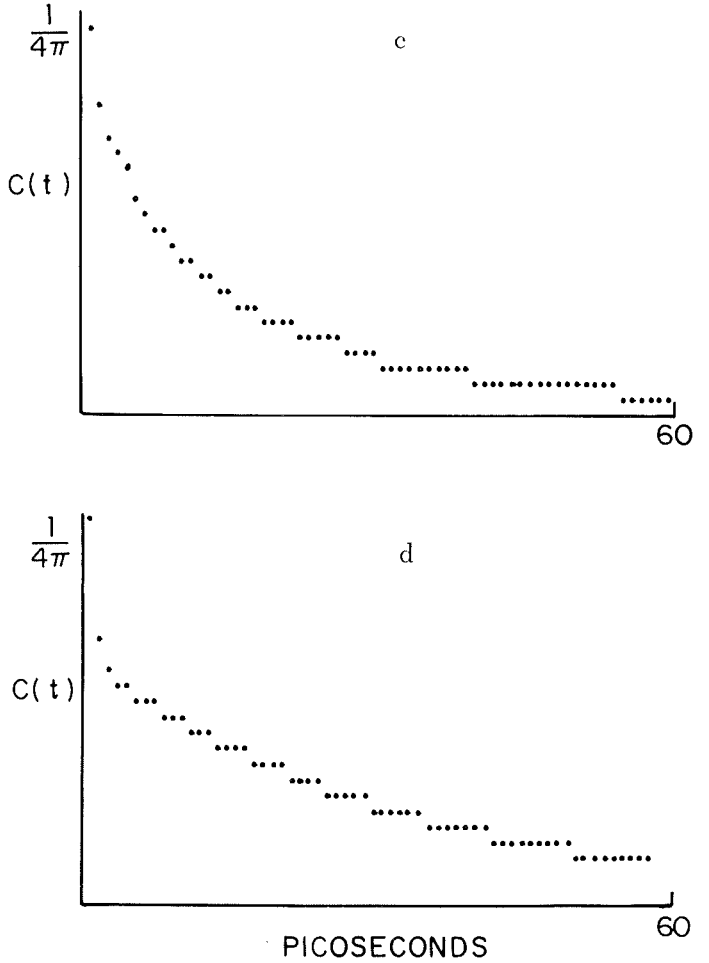

Figure 2. (continued)

culated exactly from the trajectory with the relaxation of this vector obtained when correlations between the tumbling and internal motions are broken. Also given in the figure are the separate relaxation of the tumbling and the internal motion parts of the correlation function. The first three correlation functions (Figure 2, a–c) decay to zero, but the internal motions part (Figure 2d) does not, because there is not enough freedom to sample all solid angles in this short alkane. Table IV lists the time integrals (Equation 8) of these correlation functions and the fits to them of single exponentials over several time spans. The results indicate that, for this particular carbon and choice of molecular tumbling axis,

separating the dynamics into contributions from tumbling and internal relaxation is a rather good approximation. Further analysis of the applicability of Equation 12 requires individual values for τ_0 and τ_i from the stochastic trajectory. With estimates of the tumbling and internal relaxation times of $\tau_0 \simeq 16$ ps and $\tau_i \simeq 39$ ps (*41*), the empirical relation (Equation 12) yields an estimate for the total relaxation time of $\tau_{eff} = 11$ ps, as compared with the value of $\tau_{eff} = 10$ ps obtained from a fit of the exact dynamics to a single exponential. Thus, the present trajectory results support the usefulness of the empirical relation, Equation 12. A more detailed analysis for longer hydrocarbons is in progress (*50*).

NMR Relaxation of a Side Chain Attached to a Tumbling Macromolecule

In this section, the heptane trajectory is used as outlined in the section on methodology to evaluate T_1, T_2, and NOE for a model aliphatic side chain with four internal rotational angles protruding from a tumbling macromolecule.

Exact Trajectory Results. The NMR relaxation parameters T_1, T_2, and NOE for each of the carbons (C2 through C6) calculated exactly by means of Equations 3–6 and 13 from the trajectory are listed in Table V. Results obtained for three isotropic molecular tumbling times (τ = 1 ns, 10 ns, and 100 ns) and for two spectrometer frequencies (15 MHz and 68 MHz) are compared.

Of the many comparisons that can be made with the results in Table V, we consider first the calculations for 15 MHz, $\tau_0 = 1$ ns where the NMR relaxation parameters are characteristic of the motional narrowing limit; i.e., T_1 equals T_2 for all of the carbons along the chain and the NOE value is almost maximal, even for the slowest-relaxing carbon. The NMR relaxation times for this case are inversely proportional to the time integrals of the angular correlation functions (Equations 8–10). The much more rapid decay for the C6–H vector results in a 25-fold increase in the value of T_1 over that for the C2 carbon; i.e., the fast reorientation of the C6–H vector averages out the effect of the macromolecular tumbling, which is in the frequency range to produce highly efficient relaxation (as found for C2). Thus, the internal flexibility has a dramatic effect on the NMR relaxation. This is to be contrasted with the results for the heptane chain in solution. For that system, which is also in the motional narrowing limit, the much higher tumbling rate (on the same order as the internal motions) leads to longer relaxation times and a much weaker variation of T_1 with position in the chain. It is of interest that in the macromolecule the T_1 value of C6 with its large internal motional freedom approaches that obtained for the free heptane.

To examine the contributions of internal motions to the relaxation,

Table V. Side Chain NMR Parameters, Exact Result

	15 MHz			*68 MHz*		
Tumbling Time	T_1 *(ms)*	T_2 *(ms)*	*NOE* $(1+\eta)$	T_1 *(ms)*	T_2 *(ms)*	*NOE* $(1+\eta)$
τ_0 = *1 ns*						
C2 (analytic)	26.5	25.8	2.80	58.3	48.9	1.70
C3	112	110	2.86	179	163	2.34
C4	290	290	2.97	312	308	2.90
C5	452	450	2.96	493	486	2.90
C6	627	625	2.97	682	672	2.90
τ_0 = *10 ns*						
C2 (analytic)	11.9	7.3	1.30	133	11	1.16
C3	60	40	1.63	230	57	2.44
C4	243	223	2.74	292	247	2.91
C5	368	313	2.50	492	358	2.95
C6	519	454	2.60	665	515	2.92
τ_0 = *100 ns*						
C2 (analytic)	62.4	1.2	1.16	1,270	1.2	1.15
C3	171	7.1	2.18	302	7.2	2.87
C4	274	101	2.93	293	103	2.93
C5	466	99	2.86	496	100	2.94
C6	617	163	2.89	667	165	2.94

we compare the high field (68 MHz) results at the two slower tumbling times (10 ns and 100 ns). For the rigid carbon C2, the macromolecule is tumbling too slowly for efficient relaxation; consequently, T_2, T_1 and the NOE value are minimal. Side chain flexibility can enhance relaxation rates because of the presence of additional frequency components closer to the Larmor frequency. This does not occur for the side chain tumbling at τ = 10 ns, where the increase in T_1 along the chain is monotonic. However, the micelle tumbling (100 ns) is so slow with respect to the Larmor frequency that internal motions do increase the relaxation rates. The rigid C2 carbon T_1 is longer than 1 s while C3, which can reorient about one side chain rotation axis, has a T_1 of only 302 ms. The high-field T_1 and T_2 values for C6, which is farthest out along the chain, demonstrate that T_1 is sensitive to the high frequency molecular motions, whereas T_2 probes primarily the low frequency motions. For C6, the T_1 values at τ = 10 ns and at 100 ns are almost identical (665 and 667 ms, respectively). By contrast, T_2 is much shorter for the longer tumbling time (for C6, T_2 = 515 ms at τ = 10 ns and T_2 = 165 ms at τ = 100 ns). This result demonstrates the importance of measuring both T_1 and T_2 in order to obtain information about molecular dynamics from NMR.

Simplified Models. We now evaluate the NMR parameters obtained from simplified models for the side chain dynamics and compare the results obtained from these models with the exact results. In the product approximation, motions about the side chain rotational axes are assumed to be uncorrelated. We have found, for most of the cases studied, that the NMR parameters calculated from the product approximation are close to the exact results. For example, at $\tau_0 = 1$ ns or 10 ns, the results for C4 are calculated in the product approximation to be within 5% of the exact values (*41*). Even for C6 the approximate NMR parameters are within 50% of the exact results. That the product approximation generally gives good results suggests that correlations among neighboring dihedral angles do not play a significant role in the chain isomerization dynamics.

The independent lattice jump model idealizes the chain dynamics to instantaneous jumps among stable side chain configurations; between jumps the side chain is assumed to be tumbling rigidly with the macromolecule. NMR parameters calculated from the independent lattice jump model using isomerization rate constants calculated from the heptane trajectory (*34*) are listed in Table VI. In contrast to the product

Table VI. Side Chain NMR Parameters, Lattice Jump Model

	15 MHz			*68 MHz*		
Tumbling Time	T_1 *(ms)*	T_2 *(ms)*	*NOE* $(1+\eta)$	T_1 *(ms)*	T_2 *(ms)*	*NOE* $(1+\eta)$
$\tau_0 = 1$ *ns*						
C2 (analytic)	26.5	25.8	2.80	58.3	48.9	1.70
C3	99	97	2.86	162	147	2.31
C4	226	225	2.96	252	247	2.85
C5	339	339	2.98	358	355	2.92
C6	511	510	2.98	520	518	2.97
$\tau_0 = 10$ *ns*						
C2 (analytic)	11.9	7.3	1.30	133	11	1.16
C3	52	35	1.59	216	50	2.40
C4	179	158	2.63	235	183	2.85
C5	296	278	2.81	338	301	2.92
C6	477	469	2.94	496	481	2.96
$\tau_0 = 100$ *ns*						
C2 (analytic)	62.4	1.2	1.7	1270	1.2	1.15
C3	159	6.0	2.11	295	6.1	2.88
C4	219	60	2.90	241	61	2.91
C5	324	151	2.94	339	153	2.95
C6	437	377	2.98	496	380	2.98

approximation, which yields T_1 and T_2 values that are uniformly longer than the exact results, those calculated from the jump model are uniformly shorter than the exact results. The jump model relaxation times are generally within 30% of the exact values, although the high field T_2 values for micellar tumbling (τ_0 = 100 ns) differ by 50% for C6. An important source of error introduced by the jump model is readily apparent when plots of the angular correlation functions are examined (Figure 3). The plots of the product approximation and the exact relaxation for the C6–H vector are very similar. The jump model, however, exhibits a considerably slower initial decay as compared with the two other functions. The reason for the absence of the fast initial decay in the jump model is that it does not include the high frequency, small-amplitude oscillations that occur within a given potential well. The good results obtained from the jump model in the present case are due to a cancellation of errors. Uncoupling the correlation in the motions along the chain leads to a more rapid decay (less efficient NMR relaxation), while ignoring the short time oscillations of the chain leads to a slower decay (more efficient NMR relaxation). Although these corrections are not very large for the present system, there are cases (e.g., in the interior of proteins) where jumps are so rare that the oscillations within a well make a more important contribution to the relaxation. In the following section we briefly review the results of our trajectory studies of the picosecond motional averaging of NMR probes in the protein interior.

Picosecond Motional Averaging of NMR Probes of Protein Dynamics

In spite of the close-packed structure of native proteins, molecular dynamics simulations (*51*) have shown that significant atomic fluctuations occur on a picosecond time scale. We have used a molecular dynamics simulation of the pancreatic trypsin inhibitor (PTI) to demonstrate the effects of picosecond fluctuations on the observed ^{13}C T_i values. The NMR relaxation rates are determined by time correlation functions, and these correlation functions decay on several different time scales. On the shortest time scale, there is a rapid initial loss of correlation in the first few picoseconds (*44*). The fast decay results from the combined effect of the vibrational potential of the residue containing the nucleus and of collisions between the atoms of the residue and those of the surrounding cage in the protein. For residues that are involved in larger, more complex fluctuations, the initial decay is followed by a much slower loss of correlation over the next tens to hundreds of picoseconds. If the internal motions are restricted, the correlation functions will decay to a plateau value that is equal to the inverse of the square of the order parameter

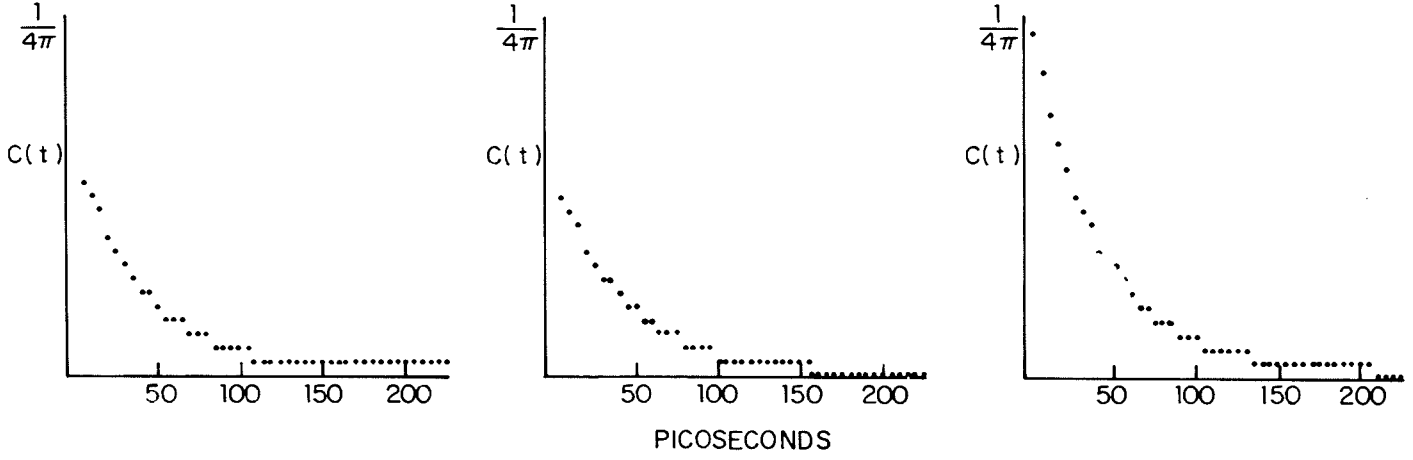

Figure 3. The C6–H angular correlation function: left, calculated exactly from the trajectory (Equation 13); center, calculated from the product approximation; and right, calculated from the independent lattice jump model (Equation 15). (Reprinted from Ref. 41. Copyright 1981, American Chemical Society.)

that describes the distribution of NMR probe orientations (Equation 16). Finally, for experiments in solution, the correlation functions relax to zero due to the overall tumbling of the proteins.

For an examination of the effect of fast motional averaging on T_1 values, we have evaluated the order parameters (Equation 16) and the increase in T_1 values (Equation 17) for 62 protonated (*44*) and 4 nonprotonated (*45*) carbons in PTI. In 13 out of 14 α-carbons studied, motional averaging increased the T_1 values by less than 20% ($1.05 \leq T_i/T_i^R \leq 1.11$). An examination of the NMR correlation functions for these atoms demonstrated that they do approach a plateau value within 2 ps. We therefore concluded that it is unlikely that lower frequency internal fluctuations contribute significantly to the relaxation of these atoms. For the 12 residues studied that have side chains, all of the β carbons exhibit more motional averaging than the α carbons to which they are attached. An approximate plateau value appears within 2 ps ($1.11 \leq T_i/T_i^R \leq 1.23$). Of all the carbons studied, the aliphatic γ carbons had the greatest increase in T_1. However, for these carbons the motional averaging does not plateau within 2 ps and lower frequency fluctuations contribute to the NMR relaxation.

The motions of aromatic side chains in proteins have been the subject of several recent experimental and theoretical investigations (*45, 52–55*). A large number of experimental techniques can be used to study the ring motions, including ^{13}C NMR relaxation, ^{1}H and ^{2}H lineshape, and fluorescence depolorization measurements. Levy et al. (*43–46*) have used molecular dynamics simulations of pancreatic trypsin inhibitor (PTI) to evaluate the picosecond motional averaging of order parameters for NMR and fluorescence probes of ring motions. In the course of this work it was observed that the order parameters were anomalously small for certain probe orientations on the two rings in PTI that flipped during the trajectory. Levy and Sheridan (*56*) subsequently developed a simple analytical model that can be used to evaluate order parameters for probes of ring motions when the rings are undergoing both restricted diffusion and 180° jumps about the side chain axes. It was demonstrated that, within the model, the restricted high frequency ring motions can have a large effect on the probe order parameters. Extension of this work to analyze the effect of restricted ring motions on NMR line-shapes in the solid state is underway.

Conclusions

Stochastic dynamics trajectories for alkanes in aqueous solution have been used to examine a variety of problems that arise in the interpretation of ^{13}C-NMR relaxation experiments. Exact results for T_1, T_2, and NOE values obtained from these trajectories have been employed to analyze

the relaxation behavior of small alkanes and macromolecular side chains and to test the validity of simplified relaxation models for these systems. Results were obtained for the spin lattice relaxation times of butane and heptane in aqueous solution. A gradient in relaxation times along the heptane chain was found that is in agreement with the measured values for the neat liquid. The empirical separation of the relaxation contributions in these molecules into a tumbling term plus an internal motion term was shown to yield useful results. We have also been able to analyze models for side chain relaxation in macromolecules. For macromolecules with short alkanelike side chains moving freely in aqueous solvent, the lattice jump model was shown to provide a satisfactory description of the NMR relaxation.

A molecular dynamics simulation of a protein has been used to demonstrate the effects of picosecond fluctuations on observed ^{13}C T_1 values. It is shown how an increase in T_1 can be related to order parameters for the picosecond motional averaging of the C, H dipolar interactions, and how these order parameters can be calculated from a protein molecular dynamics trajectory.

In summary, the present work provides a firm theoretical foundation for the continuing effort to use NMR measurements for the experimental analysis of the dynamics of molecules with internal degrees of freedom.

Acknowledgments

We thank C. M. Dobson for helpful discussion. We thank G. Lipari and A. Szabo for many discussions concerning generalized order parameters and for making preprints of their work available to us. This work has been supported by grants from the National Institutes of Health, the National Science Foundation, the Petroleum Research Fund, and the Rutgers University Research Council and a Biochemical Research Support Grant. R. M. Levy is an Alfred P. Sloan Fellow and the recipient of a National Institutes of Health Research Career Award.

Literature Cited

1. Kuhlman, K.; Grant, D.; and Harris, R. *J. Chem. Phys.* **1970**, *52*, 3439.
2. Lyerla, J. R., Jr.; Grant, D. *J. Phys. Chem.* **1972**, *76*, 3213.
3. Bauer, D.; Alms, G.; Brauman, J.; Pecora, R. *J. Chem. Phys.* **1974**, *61*, 2255.
4. Lyerla, J. R.; Levy, G. C. *Top. Carbon–13 NMR Spect.* **1974**, *1*, 79.
5. Jonas, J. *Proc. Nato ASI High Press. Chem.* **1978**, Reidel, Dordrecht.
6. Doddrell, D.; Allerhand, A. *J. Am. Chem. Soc.* **1971**, *93*, 1558.
7. Connor, T. M. *J. Chem. Soc., Trans. Faraday* **1963**, *60*, 1579.
8. Schaefer, J. *Macromolecules* **1973**, *6*, 882.
9. Levine, Y. K.; Birdsall, N.; Lee, A. G.; Metcalfe, J. C.; Partington, P.; Roberts, G. C. K. *J. Chem. Phys.* **1974**, *60*, 2890.

10. Lyerla, J. R., Jr.; McIntyre, H. M.; Torchia, D. A. *Macromolecules* **1974**, *7*, 11.
11. Lyerla, J. R., Jr.; Horikawa, T. T. *J. Phys. Chem.* **1976**, *80*, 1106.
12. Levy, G. C.; Axelson, D. E.; Schwartz, R.; Hochmann, J. *J. Am. Chem. Soc.* **1978**, *100*, 410.
13. Canet, D.; Brondeau, J.; Nery, H.; Marchol, J. P. *Chem. Phys. Lett.* **1980**, *72*, 184.
14. Lee, A. G.; Birdsall, N. J. M.; Metcalfe, J. E.; Warren, G. B.; Roberts, G. C. K. *Proc. Roy. Soc. Lond.* **1976**, *193B*, 253.
15. Godini, P.; Landsberger, F. *Biochemistry* **1975**, *14*, 3927.
16. Bocian, D.; Chan, S. *Annu. Rev. Phys. Chem.* **1978**, *29*, 307.
17. Oldfield, E.; Norton, R.; Allerhand, A. *Biochemistry* **1975**, *250*, 6338.
18. *Ibid.*, **1975**, *250*, 6381.
19. Visscher, R.; Gurd, F. R. N. *J. Biol. Chem.* **1975**, *250*, 2238.
20. Jones, W. C., Jr.; Rothgeb, T. M.; Gurd, F. R. N. *J. Biol. Chem.* **1976**, *251*, 7452.
21. Wittebort, R. J.; Rothgeb, T. M.; Szabo, A.; Gurd, F. R. N. *Proc. Nat. Acad. Sci. USA* **1979**, *76*, 1059.
22. Jelinski, L. W.; Torchia, D. *J. Mol. Biol.* **1979**, *133*, 45.
23. Jelinski, L. W.; Torchia, D. *J. Mol. Biol.* **1980**, *138*, 255.
24. Wallach, D. *J. Chem. Phys.* **1967**, *47*, 5258.
25. Wittebort, R. J.; Szabo, A.; Gurd, F. R. N. *J. Am. Chem. Soc.* **1980**, *102*, 5723.
26. Wittebort, R. J.; Szabo, A. *J. Chem. Phys.* **1978**, *69*, 1722.
27. London, R. E.; Avitable, J. *J. Am. Chem. Soc.* **1978**, *100*, 7159.
28. Howarth, O. W. *J. Chem. Soc., Faraday Discuss. II*, **1979**, *75*, 863.
29. London, R. E.; Avitable, J. *J. Am. Chem. Soc.* **1977**, *99*, 7765.
30. Tsutsumi, A.; Chachaty, C. *Macromolecules* **1979**, *12*, 429.
31. Chandrasekhar, S. *Rev. Mod. Phys.* **1943**, *15*, 1.
32. Ermak, D. L.; McCammon, J. A. *J. Chem. Phys.* **1978**, *69*, 1352.
33. Ermak, D. L.; *J. Chem. Phys.* **1975**, *62*, 4189.
34. Levy, R. M.; Karplus, M.; McCammon, J. A. *Chem. Phys. Lett.* **1979**, *65*, 4.
35. Ryckaert, J. P.; Cicotti, G.; Berendsen, H. J. C. *J. Comp. Phys.* **1977**, *23*, 327.
36. Ryckaert, J. P.; Bellemans, A. *Chem. Phys. Lett.* **1975**, *30*, 123.
37. Pratt, L. R.; Chandler, D. *J. Chem. Phys.* **1977**, *67*, 3683.
38. Fixman, M. *J. Chem. Phys.* **1978**, *69*, 1527.
39. Levy, R. M.; In "Stochastic Molecular Dynamics"; National Resources for Computation in Chemistry; Lawrence Berkeley Laboratory, Univ. CA, Berkeley; 1979.
40. Abragam, A. "The Principles of Nuclear Magnetism"; Oxford Press: London, 1978.
41. Levy, R. M.; Karplus, M.; Wolynes, P. G. *J. Am. Chem. Soc.* **1981**, *103*, 5998.
42. Berne, B.; Pecora, R. "Dynamic Light Scattering"; Wiley: New York, 1976; Chap. 7.
43. Levy, R. M. In "Diffusive Dynamics of Alkane Chains"; CECAM Workshop Report, Universite de Paris, 1978.
44. Levy, R. M.; Karplus, M.; McCammon, J. A. *J. Am. Chem. Soc.* **1981**, *103*, 994.
45. Levy, R. M.; Dobson, C. M.; Karplus, M. *Biophys. J.* **1982**, *39*, 107.
46. Levy, R. M.; Szabo, A. *J. Am. Chem. Soc.*, **1982**, *104*, 2073.

47. Bocian, D. F.; Chan, S. I. *Ann. Rev. Phys. Chem.* **1979,** *29,* 307.
48. Lipari, G.; Szabo, A. *J. Am. Chem. Soc.* in press.
49. Knauss, D. C.; Evans, G. T.; Grant, D. M. *Chem. Phys. Lett.* **1980,** *71,* 158.
50. Pastor, R.; Karplus, M.; Levy, R. M. to be submitted for publication.
51. Karplus, M.; McCammon, J. A. *CRC Crit. Rev. Biochem.* **1981,** *9,* 293.
52. Campbell, I. D.; Dobson, C. M.; Moore, G. R.; Perkins, S. J.; Williams, R. J. P. *FEBS Lett.* **1976,** *70,* 91.
53. Lakowicz, J. R.; Weber, G. *Biophys. J.* **1980,** *32,* 591.
54. Gelin, B. R.; Karplus, M. *Proc. Nat. Acad. Sci.* **1975,** *81,* 801.
55. McCammon, J. A.; Wolynes, P. G.; Karplus, M. *Biochemistry* **1979,** *18,* 927.
56. Levy, R. M.; Sheridan, R. P. *Biophys. J.* in press.

RECEIVED for review March 15, 1982. ACCEPTED for publication September 13, 1982.

Reprinted from ACS ADVANCES IN CHEMISTRY SERIES, No. 204
MOLECULAR-BASED STUDY OF FLUIDS
J. M. Haile and G. A. Mansoori, Editors
Copyright 1983 by the American Chemical Society
Reprinted by permission of the copyright owner